HHS Public Access

Author manuscript

Mol Pharm. Author manuscript; available in PMC 2021 April 06.

Published in final edited form as:

Mol Pharm. 2020 April 06; 17(4): 1139–1147. doi:10.1021/acs.molpharmaceut.9b01181.

Detecting TRA-1–60 in Cancer via a Novel Zr-89 Labeled ImmunoPET Imaging Agent

Jordan M. White, **Akhila N. Kuda-Wedagedara**
Department of Oncology, Karmanos Cancer Institute, Detroit, Michigan 48201, United States

Madison N. Wicker,
Department of Biology, University of Michigan – Flint, Flint, Michigan 48502, United States

Daniel E. Spratt,
Department of Radiation Oncology, University of Michigan, Ann Arbor, Michigan 48109, United States

William M. Schopperle
CureMeta LLC, Boston, Massachusetts 02210, United States

Elisabeth Heath, **Nerissa T. Viola**
Department of Oncology, Karmanos Cancer Institute, Detroit, Michigan 48201, United States

Abstract

TRA-1–60 (TRA) is a cell-surface antigen implicated in drug resistance, relapse, and recurrence. Its expression has been reported in breast, prostate, pancreatic, ovarian tumors, and follicular lymphoma, which paved the development of the therapeutic antibody, Bstrongomab (Bsg), and its drug conjugates. Because patient selection is critical to achieve clinical benefit, a noninvasive imaging agent to select TRA+ lesions in patients is needed. Herein, we report the development of the immunopositron emission tomography (immunoPET) radiotracer ^{89}Zr-radiolabeled Bsg and its potential to delineate TRA+ tumors. Bsg was conjugated to the bifunctional chelator desferrioxamine (DFO) and radiolabeled with [^{89}Zr]Zr-oxalate. [^{89}Zr]Zr-DFO-Bsg was characterized *in vitro* and evaluated *in vivo* for uptake and specificity in high and low TRA-expressing BxPC-3 pancreatic and PC-3 prostate cancer models, respectively. Uptake was compared against[^{89}Zr]Zr-DFO-IgG, a nonspecific control radiotracer. Immunohistochemical (IHC) staining of patient cancer tissues using Bsg was performed to explore its clinical

Corresponding Author: **Nerissa T. Viola** – Department of Oncology, Karmanos Cancer Institute, Detroit, Michigan 48201, United States; Phone: (313)5768309; violan@karmanos.org; Fax: (313)5768928.

Author Contributions

JMW, AKW, and MNW performed experiments. JMW, AKW, MNW, and NTV analyzed data. JMW, AKW, WES, DES, EH, and NTV wrote the manuscript. WES, EH, and NTV conceptualized the studies. All authors edited and reviewed the manuscript before submission.

Supporting Information

The Supporting Information is available free of charge at https://pubs.acs.org/doi/10.1021/acs.molpharmaceut.9b01181.
Western blot tumor lysate TRA expression; [^{89}Zr]Zr-DFO-Bsg iTLC, immunoreactivity, binding and stability; *ex vivo* tumor HE and IgG autoradiography; negative control normal human tissues IHC; table of [^{89}Zr]Zr-DFO-Bsg internalization; tables comparing organ uptake for [^{89}Zr]Zr-DFO-Bsg and [^{89}Zr]Zr-DFO-IgG; biodistribution organ uptake tables (PDF)

Complete contact information is available at: https://pubs.acs.org/10.1021/acs.molpharmaceut.9b01181

The authors declare the following competing financial interest(s): William M. Schopperle has ownership in CureMeta LLC. Daniel E. Spratt is on the advisory board for Blue Earth and Janssen. No other potential conflicts of interest relevant to this article exist.

significance. A specific activity of 0.18 ± 0.01 GBq/mg (4.8 ± 0.3 mCi/mg) was obtained for [^{89}Zr]Zr-DFO-Bsg. BxPC-3 xenografts exhibited three-fold higher radiotracer uptake compared to [^{89}Zr]Zr-DFO-IgG. Competitive saturation studies using BxPC-3 xenografts further confirmed tracer specificity. The TRA-specific probe had lower accumulation in PC-3 xenografts. *Ex vivo* autoradiographs correlated with TRA expression from the histopathology of the resected tumor xenografts. Additionally, patient cancer tissues demonstrated positive staining with Bsg with metastatic lesions exhibiting the highest staining. This study demonstrates the potential of [^{89}Zr]Zr-DFO-Bsg as an imaging agent for noninvasive detection of TRA+ tumors.

Graphical Abstract

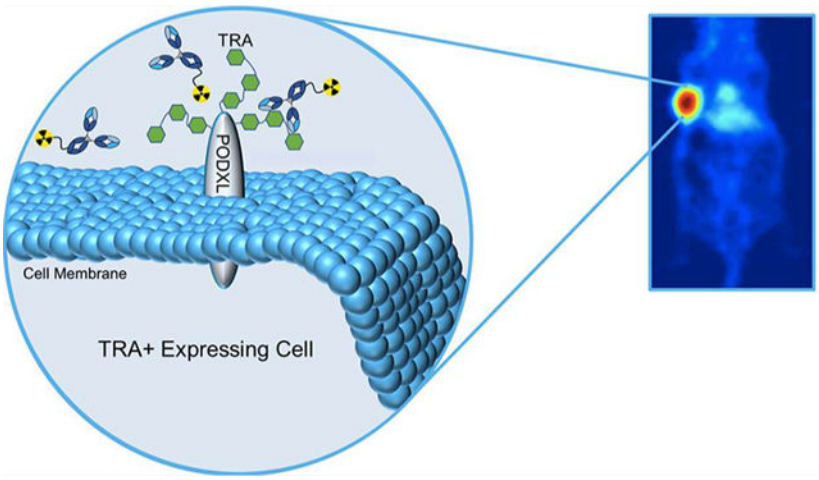

Keywords

immunopositron emission tomography; TRA-1–60; tumor initiating cells; metastasis

INTRODUCTION

Tumors comprise a diverse population of cells that contributes to their heterogeneity. One particular phenotype possesses tumor-initiating potential and was proposed to drive treatment resistance, relapse, and metastasis.[1–4] Its identification within the tumor can potentially provide prognostic information and inform treatment decisions. Putative signatures observed solely on these tumor-initiating cells have been reported. One antigen that has gained traction as a marker of malignancy and therapy resistance is TRA-1–60 (TRA),[5,6] an established biomarker of pluripotent stem cells.[7–9] TRA was discovered by Andrews et al. on the surface of treatment refractory human embryonal carcinoma.[10] It was characterized as a high molecular weight glycoprotein[11,12] localized on the surface of the transmembranous protein podocalyxin (PODXL).[8,11,12] The exact molecular structure of TRA antigen has been controversial. One group identified TRA-1–60-specific antibodies targeting sialylated keratan sulfate proteoglycans,[13] while others investigated different antibody clones that targeted a type-1 lactosamine epitope.[7]

TRA is expressed in cancer or when applicable, in metastatic lesions, including follicular lymphoma, teratocarcinoma, breast, prostate, pancreatic, ovarian, and testicular cancers.[5,14–16] In testicular cancer, TRA was shed in patient sera and presented with elevated levels, suggesting its potential use as a serum marker for patients with germ cell tumors.[17] A study conducted in treatment-refractory follicular lymphoma observed the association of TRA expression in cell populations that displayed a resistance phenotype to rituximab and other chemotherapies.[5] The same study reported greater tumor-initiating capabilities of sorted TRA+ follicular lymphoma versus negative cells. This recapitulates the findings observed by Rajasekhar et al. in prostate cancer where TRA+ sorted cells implanted in mice developed tumors over time.[5,14] Of note, a salient retrospective study by Heath et al. demonstrated that TRA was highly expressed in a small percentage of high grade prostatic tumors, suggesting a correlation between localized prostate cancer that would progress to metastatic disease.[9] These previous findings advocate the unique appeal of TRA as a biomarker and drug target due to its implication in resistance, and recurrence.[6,8,18–20]

The therapeutic IgGκ antibody Bstrongomab (Bsg) and its drug conjugates (Curemeta, LLC) were specifically developed to target TRA. The marginal presence of tumor-initiating and therapy resistant cells with TRA expression warrants a highly sensitive companion diagnostic to select patients who will benefit from Bsg-related therapies. Identification of TRA+ therapy resistant cells via immunopositron emission tomography (immunoPET) will bridge this clinical need and identify potential tumor responders for TRA inhibition. In this study, we report the preclinical evaluation of a TRA-specific immunoPET imaging agent, 89Zr-radiolabeled Bstrongomab ([^{89}Zr]Zr-DFO-Bsg), to differentiate high to low-expressing TRA tumors using pancreatic BxPC-3 and prostate PC-3 xenografts, respectively, through *in vitro*, *in vivo*, and *ex vivo* studies. The presence and levels of TRA expression in these cancers were examined and validated through confocal imaging, single cell imaging flow cytometry, and Western blots. We compared tumor uptake of [^{89}Zr]Zr-DFO-Bsg against a ^{89}Zr-labeled nonspecific isotype IgG control through *in vivo* PET imaging. Pharmacokinetic studies in tumor-bearing mice assessed tissue distribution and clearance of the tracer. Competitive inhibition with excess unmodified Bsg was performed to assess the tracer's specificity. We then analyzed the spatial localization of the radiotracer through *ex vivo* autoradiography and correlated it against TRA expression via immunohistochemistry (IHC) in BxPC-3 tissue sections. Finally, patient tumor and normal tissue samples were stained with Bsg to investigate the potential clinical application of the tracer.

EXPERIMENTAL SECTION

Imaging Cytometry.

To assess the presence of TRA on the cell surface, live BxPC-3 cells were imaged via the Amnis ImageStream X Mark II Imaging Cytometer. The cells were incubated with anti-TRA-1–60-AF488 (1:200, Cat. No. sc-21705, Santa Cruz Biotechnology). Following incubation, cells were centrifuged for 5 min at 3000 rpm, media were aspirated, and the cells were washed twice to remove unbound anti-TRA-1–60-AF488 with 1× phosphate buffered saline (PBS). Following the final wash, cells were resuspended in a concentration of 2×10^7 cells/mL in FACS buffer (7% FBS in 1× PBS) and imaged on the cytometer.

Conjugation of Bsg to Near-Infrared Dye Cyanine 5.5 (Cy5.5).

Bsg was also conjugated to a Cyanine-5.5 Mono-NHS Ester (Cy5.5, GE Healthcare Cat. No. PA15601) at a 1:5 antibody/fluorophore mole ratio for confocal imaging. Excess unbound Cy-5.5 was removed by centrifugal filtration with a 30 kDa MWCO at 3000 rpm and 15 min increments until the flow through was colorless.

Western Blot.

The expression of TRA in *ex vivo* tumor lysates was determined via Western blots as previously described.[21] Briefly, proteins were extracted from BxPC-3, DU-145, and PC-3 tumors that were mechanically homogenized with a Polytron PT1200E mechanical homogenizer (Kinematica Inc.) in 1× RIPA lysis buffer and HALT protease and phosphatase inhibitors (ThermoFisher). Tumor lysates (20 μg) were resolved on 4–12% SDS-PAGE, transferred to immobilon-P PVDF (Millipore Sigma) membrane, and blocked with 5% milk in TBS with 0.1% Tween-20. The membrane was then incubated with anti-TRA-1–60 (1:200, Santa Cruz Biotechnology sc-21705), Bsg (1:200, Curemeta), or anti-GAPDH (Santa Cruz Biotechnology Cat. No. sc-365062) overnight at 4 °C. Blots were then incubated with antimouse horse radish peroxidase (HRP) secondary antibody (Amersham Cat. No. NA931 V), visualized with Amersham ECL (GE Life Sciences), and read with a Bio-Rad ChemiDoc imaging system. Western Blot analysis was conducted with Bio-Rad image lab software 2.2.

Bsg Conjugation to Desferrioxamine (DFO).

Bsg and a nonspecific IgG isotype were conjugated to p-isothiocyanatobenzyl-desferrioxamine (DFO), a common chelator of ^{89}Zr, at a 1:5 antibody/DFO mole ratio (Macrocyclics, Inc.) via terminal lysines. DFO (33 nmol of 20 mM stock in dimethyl sulfoxide) was added to Bsg (6.6 nmol) in 1× PBS adjusted to pH ~ 8.5–9 with 1 M $NaHCO_3$.[22,23] The solution was incubated at 37 °C for 1.5 h. Following incubation, unbound DFO was removed using centrifugal filtration at 3000 rpm for 10 min using a 30 kDa molecular weight cutoff centrifugal filter (MWCO, Vivaspin V-500, Sartorius Stedim Biotech). Purification was performed in triplicate using saline as eluent.

^{89}Zr Radiolabeling of Bsg.

[^{89}Zr]Zr-oxalate (74 MBq, 2 mCi, 3D Imaging, LLC.) was diluted in saline (200 μL) and adjusted to pH ~7.0–7.5 with 1 M Na_2CO_3 and 1 M HCl in metal-free water. Bsg-DFO (0.4 mg, 2.67 nmol) was added to the solution containing the radioisotope for a final concentration of 13.33 μM and incubated for 15–20 min at room temperature.[22,24] After completion of labeling, 5 μL of 50 mM EDTA was added to quench the reaction. [^{89}Zr]Zr-DFO-Bsg was purified using a centrifugal filter (30 kDa MWCO, Vivaspin V-500) at 3000 rpm for 10 min with saline as the eluent; centrifugal purification was conducted in triplicate. Radiochemical purity was analyzed by radio-instant thin layer chromatography (radio-iTLC) using a silica gel impregnated chromatography paper (Agilent Technologies) as solid phase and 50 mM EDTA as the mobile phase. [^{89}Zr]Zr-DFO-Bsg immunoreactivity was assessed in triplicate with highly TRA+ NCCIT embryonal carcinoma, by linear extrapolation, as previously described.[25]

Accessible DFO Chelates on Bsg.

The number of chelates of DFO attached to Bsg was assessed by radiometric isotopic dilution with an adapted method similar to those previously described.[26,27] A stock solution of [^{89}Zr]Zr-oxalate was prepared, and aliquots of 660 kBq (18 μCi) was added to 13 serial dilutions (1:2) of 50 μL of nonradioactive $ZrCl_4$ from 49 nM to 200 μM at a pH = 7. [^{89}Zr]Zr-oxalate and $ZrCl_4$ were mixed for 30 s before addition of DFO-Bsg (0.07 nmol, 10.5 μg), then briefly vortexed. The reaction was incubated at room temperature for 1 h and quenched with 10 μL, 50 mM EDTA (pH 7). The extent of radiolabeling was assessed by counting the activity at the baseline and solvent front with a gamma counter (PerkinElmer Wizard^2 2480). Control radiolabeling studies confirmed [^{89}Zr]Zr-DFO-Bsg radiolabeling in <1 h.

Confocal Imaging.

To examine the specificity of Bsg, BxPC-3 cells (2.5×10^4) were plated on a Millicell EZ Slide. After 48 h, cells were incubated at 37 °C with TRA-1–60-AF488, Bsg-Cy5.5 (1:200) or both. A separate group of plated cells was incubated in media without TRA-1–60-AF488 or Bsg-Cy5.5 and used as control. Cells were then fixed with 4% paraformaldehyde, stained with DAPI, and imaged with a Zeiss LSM 780 confocal microscope at 63×.

Internalization Assay.

Lysine coated 12-well plates (Corning Cat. No. 354470) were seeded with 150 000 NCCIT cells and allowed to adhere overnight. The cells were then incubated with radiolabeled [^{89}Zr]Zr-DFO-Bsg (100 ng, 0.3 μCi, 111 kBq) in 0.5 mL of medium at 37 °C for 6 h, 24 h, 48 h, and 72 h. Following incubation, the media were collected, and the cells were washed twice with 1 mL of 1× PBS. Next, cells were washed with cold 100 mM acetic acid + 100 mM glycine (1:1 in PBS, pH 3–3.5) to remove the membrane bound activity. To assess internalized activity, cells were lysed with 1 M NaOH. The washes were collected and measured using a gamma counter (PerkinElmer Wizard^2 2480). The percent of membrane bound and internalized acitivity was calculated as the fraction of the total activity from all washes.

Determination of Dissociation Constant (K_D) and Maximum Binding (B_{max}) of [^{89}Zr]Zr-DFO-Bsg.

The K_D and B_{max} values were determined through an *in vitro* binding assay. NCCIT embryonal carcinoma cells were plated at 200 000 cells/well in a poly-D-lysine coated clear 12-well plate (Corning, Cat. No. 354470) and allowed to adhere for 24 h at 37 °C and 5% CO_2. The cells were either incubated with 0.62–50 nM of [^{89}Zr]Zr-DFO-Bsg or subjected to blocking by coincubation of 0.62–50 nM of [^{89}Zr]Zr-DFO-Bsg with >80-fold excess nonradiolabeled Bsg in triplicate for 1 h at room temperature. Following incubation, the media were removed, and cells were washed twice with 1× PBS, detached with 0.25% trypsin-EDTA, and collected in microcentrifuge tubes. The radioactivity of the samples and concentration standards were measured with a gamma counter (PerkinElmer Wizard^2 2480) and plotted as sites/cell versus antibody concentration (nM). GraphPad Prism was used to determine the K_D and B_{max} with a one-site association curve.

[^{89}Zr]Zr-DFO-Bsg Stability in Saline.

To assess the stability of the antibody *in vitro*, 9.25 MBq of [^{89}Zr]Zr-DFOBsg (250 μCi, 0.33 nmol) was incubated in 0.9% NaCl (saline) at 37 °C with gentle mixing following a published protocol.[28] The stability was monitored between 4 and 144 h post-incubation using radio-iTLC and reported as the ratio of the bound activity to total activity calculated from the area under the curve using Graphpad Prism.

Cell Lines and Small Animal Xenografts.

All animal experiments were conducted in accordance with the guidelines set forth by the Wayne State University Institutional Animal Care and Use Committee (IACUC) and the Division of Laboratory Animal Resources (DLAR). All cell lines unless otherwise state were purchased from ATCC (Manassas, VA). The NCCIT embryonal carcinoma cells (provided by Curemeta, LLC) are highly positive for TRA and used for confirmatory control studies. All cells were cultured at 37 °C at 5% CO_2 using aseptic technique with RPMI-1640 media containing 10% FBS (v/v) and 1% penicillin/streptomycin (v/v). L-Glutamine (1% v/v, Corning Cellgro) was added to supplement the growth media for the PC-3 cells. For imaging and biodistribution studies, BxPC-3 and PC-3 xenografts (5×10^6 cells) were established (1:1 media:Matrigel, Corning, Cat. No. 354428) subcutaneously (s.c.) on the shoulder of female and male, athymic nude mice, respectively (Envigo). Tumor growth was monitored until volumes reached 150–200 mm^3 and calculated according to the equation $V = L \times W \times H \times \pi/6$.

PET Imaging Experiments.

Mice bearing either BxPC-3 or PC-3 ($n = 3$–4) xenografts were randomly selected for PET imaging with [^{89}Zr]Zr-DFO-Bsg or [^{89}Zr]Zr-DFO-IgG. Each tracer (7.4–9.4 MBq, 200–250 μCi, 40–50 μg) was administered intravenously (i.v.) in separate mice followed by image acquisition (Siemens Concord microPET R4 or Focus 220) at 4–120 h postinjection (p.i.) while anesthetized with 2% isoflurane (Henry Schein) in oxygen. Following 120 h p.i., mice were euthanized via CO_2 asphyxiation, and death was assured by cervical dislocation. The PET images were reconstructed via filter back projection, and volumes of interest (VOIs) were measured with ASIPro VM software version 6.3.3.0 (Concorde Microsystems). VOIs were measured by manually drawing regions of the tumor on multiple planes and expressed as % injected dose per gram of tissue (%ID/g).

Tissue Biodistribution Studies.

A separate cohort of mice bearing tumors ($n = 5$) was administered i.v. in the lateral tail vein with 0.74–1.48 MBq (20–40 μCi, 4–8 μg) of [^{89}Zr]Zr-DFO-Bsg. A competitive inhibition study was conducted in a separate group of mice by coadministration of the radiotracer and ~500 μg of nonradiolabeled Bsg-DFO ($n = 5$). Mice were euthanized by CO_2 asphyxiation after 24, 48, 72, and 120 h p.i. Wet weights of the harvested tissues, including the tumor, were obtained. Bound activity was measured via a gamma counter (PerkinElmer Wizard^2 2480), decay-corrected to the time of injection and presented as %ID/g or% ID.

Autoradiography and Immunohistochemistry.

After PET imaging, autoradiographs were obtained from excised frozen sections of BxPC-3 tumors separately administered with [^{89}Zr]Zr-DFO-Bsg and [^{89}Zr]Zr-DFO-IgG. BxPC-3 tumors were excised and embedded in optimal-cutting-temperature mounting medium (OCT, Sakura Finetek) then frozen gradually on dry ice. Digital autoradiography was performed by exposing tissue sections (5 μm thick) and activity standards to a phosphor imaging plate (Fujifilm BAS-MS2325; Fuji Photo Film) at −20 °C overnight. Phosphor plates were read with a Typhoon 7000 IP plate reader (GE Healthcare) at a 25 μm resolution. High and low points of localized tracer uptake were measured by fixed size regions-of-interest (ROI) within the outlined area for Bsg and IgG using calibration standards.

IHC was performed on sequential sections to demonstrate the specificity of the radiotracer. Adjacent sections were fixed with ice-cold acetone for 10 min, dried at room temperature for 20 min, then rehydrated with PBS. Tissue sections were blocked with protein block (Abcam) at room temperature for 1 h and incubated with TRA-1–60 (sc-21705, Santa Cruz Biotechnology, 1:100) for 1 h at room temperature. Slides were developed using a mouse- and rabbit-specific HRP/DAB (ABC) detection IHC kit (Abcam Cat. No. ab64264,), dehydrated with 70–100% ethanol, followed by incubation with xylene and covered with Permount mounting medium (Fisher Chemical Cat No. SP15–500). The tissues were then imaged at 40× with Leica SCN400 SL801 Slide Scanner (Leica Microsystems).

Matching areas of IHC tissues were quantified with ImageJ software by color deconvolution using the H DAB protocol. A correlation between tracer uptake using the autoradiographs and TRA expression was determined by measuring expression and tracer uptake of the aforementioned measured areas.

Patient IHC Staining and Analysis.

Tissues obtained from US Biomax (Derwood, MD) were formalin-fixed, paraffin embedded, and sectioned at 5 μm. The sections were then deparaffinized, rehydrated in water, and prepared by heat-induced antigen retrieval by Diva Decloaker (Biocare Medical Cat. No. DV2004MX), and Decloaking Chamber (Biocare Medical). Sections were stained with Bsg (1 mg/mL, 1:500) or Mouse IgG1κ isotype control antibody (Biolegend Cat. No. 401407, 1:500) by using PowerVision+ poly-HRP IHC detection systems (Leica Cat. No.PV6106).

Statistical Analysis.

Statistical analyses were conducted with a one-way ANOVA with Tukey post test unless otherwise noted. *Ex vivo* autoradiography ROI values were compared with a nonparametric *t* test. Correlation of IHC to autoradiographs was conducted by a two-tailed Spearman r correlation. All analyses were conducted using GraphPad Prism 7.03. All values are reported as mean ± SD. In all tests, a p-value of ≤ 0.05 was considered statistically significant.

RESULTS

In Vitro and *Ex Vivo* Assessment of TRA Expression and Bsg Binding.

Western blot analysis of TRA using Bsg as the detecting antibody displayed the highest expression in BxPC-3, followed by DU-145, while PC-3 showed minimal TRA expression (Figure S1A, left). A separate Western blot using a commercial TRA-1–60 antibody (mAb) validated these results (Figure S1A, right).

Single cell imaging using an imaging flow cytometer stained with anti-TRA-1–60-AF488 was utilized to demonstrate *in vitro* localization of the antigen in BxPC-3 (Figure 1A). Confocal images of BxPC-3 cells incubated with anti-TRA-1– 60-AF488 (Figure 1B) and Bsg-Cy5.5 (Figure 1C, Figure S1B) demonstrated extracellular cell surface staining. No staining was observed in the negative control cells (Figure S1C).

Radiosynthesis, Characterization, and *In Vitro* Stability of [^{89}Zr]Zr-DFO-Bsg.

Optimized [^{89}Zr]Zr-labeling of Bsg-DFO ([^{89}Zr]Zr-DFO-Bsg) was achieved by titrating Bsg-DFO with different mole ratios of [^{89}Zr]Zr-oxalate. A final specific activity of 0.18 ± 0.01 GBq/mg (4.8 ± 0.3 mCi/mg) with a > 99% radiochemical purity was obtained (Figure S2A). The immunoreactivity of [^{89}Zr]Zr-DFO-Bsg toward TRA-1–60 was retained at 67.0 ± 1.7% (Figure S2B). Radiometric isotopic dilution assays (n = 3) determined an average of 5.3 ± 0.8 accessible chelates per mAb. *In vitro* competitive binding of varied concentrations of [^{89}Zr]Zr-DFO-Bsg with excess cold Bsg in NCCIT cells demonstrated a dissociation constant (K_D) of 2.0 ± 0.4 nM with a B_{max} = 6303.5 ± 389.6 sites/cell (Figure S2C).

We next examined the ability of [^{89}Zr]Zr-DFO-Bsg to internalize with the high TRA-expressing NCCIT cell line. The membrane bound fraction remained consistent over 72 h, whereas an increase in the internalized fraction was observed (Figure 1D, Table S1).

The stability of the [^{89}Zr]Zr-DFO-Bsg complex was assessed *in vitro* by incubating the tracer at 37 °C in 0.9% saline. After 24 h of incubation, the tracer remained intact (98.7 ± 1.2%) when compared to bound fractions at the start of the incubation (99.7 ± 0.4%). Minimal demetalation was observed at 48 h (95.2 ± 0.1%). The intact tracer fraction, however, decreased at 72 h (90.3 ± 5.6%); this plateaued over time (89.9 ± 2.9% at 96 h; 90.7% ± 4.4% at 120 h; and 88.7 ± 4.7% at 144 h) (Figure S2D).

[^{89}Zr]Zr-DFO-Bsg PET Imaging Identified Distinct TRA Tumor Expression.

In vivo PET images of BxPC-3 tumor-bearing mice exhibited tracer uptake (Figure 2A) within 4 h (4.1 ± 0.4%ID/g), which increased by three-fold at 24 h p.i. (12.2 ± 2.0%ID/g) (Table S2). The tracer uptake was retained between 48 h and 120 h p.i. (48 h: 15.4 ± 2.0% ID/g; 72 h: 15.4 ± 2.4% ID/g; 120 h: 17.0 ± 2.4%ID/g). A plot of radioactivity accumulation (Figure 2B, Table S2) in select organs displayed decreasing liver (the main route of excretion[29]) and blood (using VOIs drawn on the heart) tracer binding over time. To determine tumor-specific uptake of [^{89}Zr]Zr-DFO-Bsg *in vivo*, we compared the tracer versus a ^{89}Zr-labeled nonspecific IgG isotype control. Tumor binding of [^{89}Zr]Zr-DFO-IgG

was significantly lower compared to the TRA-specific tracer throughout all time points ($p < 0.0001$, Figure 2C, Table S2).

In low TRA-expressing PC-3 xenografts, the tumor uptake of [^{89}Zr]Zr-DFO-Bsg was constant throughout the imaging experiment (4 h, 5.8 ± 0.9%ID/g; 24 h, 7.0 ± 1.1%ID/g; 48 h, 6.9 ± 1.1%ID/g; 72 h, 7.4 ± 1.0%ID/g; 120 h, 6.5 ± 1.3% ID/g, Figure 2D, Table S3) and was not significantly different from the [^{89}Zr]Zr-DFO-IgG uptake (Figure 2F, Table S3). Tracer binding and retention in blood, liver, and muscle (Figure 2E, Table S3) remained similar to the BxPC-3 tumor model. From this study, [^{89}Zr]Zr-DFO-Bsg was able to measure and identify tumors with varying TRA expression.

Tissue Biodistribution.

Acute tissue distribution studies were conducted in mice-bearing BxPC-3 tumors at 24–120 h p.i. Tumor uptake at 24 h p.i. was measured at 12.6 ± 2.7%ID/g (Figure 3, Table S4). The maximal accumulation occurred at 48 h p.i. at 19.3 ± 2.4%ID/g. The probe was retained in the tumor at 72 h (13.5 ± 3.5%ID/g) and 120 h (15.5 ± 8.1%ID/g). Blood pool residency at 24 h p.i. was measured at 29.8 ± 4.5%ID/g, which continued to decrease over time. Nonspecific binding of the tracer in other normal tissues (e.g., stomach, brain, bone, and muscle), especially in the pancreas, was minimal throughout all time points with <2%ID/g. A blocking study in a separate cohort of mice was conducted with coinjection of ~500 μg of nonradiolabeled Bsg together with the radiotracer (4–8 μg, 20–40 μCi) and assessed at 72 h p.i. Not accounting for tumor weights, the uptake of the nonblocked groups (8.4 ± 3.0%ID) was 6.7-fold higher than the blocked cohort (Figure 3, inset, Table S5) (1.3 ± 0.7%ID, $p = 0.011$).

Ex Vivo Autoradiography Correlates with TRA Immunohistochemical Expression.

Ex vivo autoradiographs from tumors excised postimaging were obtained to determine spatial localization of the tracer *vis-à-vis* TRA IHC. [^{89}Zr]Zr-DFO-Bsg exhibited heterogeneous but focal tissue localization (Figure 4A, Figure S3A), whereas [^{89}Zr]Zr-DFOIgG was observed to accumulate within the tumor periphery (Figure S3B). Quantification of both bound tracers displayed a higher accumulation of [^{89}Zr]Zr-DFO-Bsg in different regions (ROIs) compared to [^{89}Zr]Zr-DFO-IgG (1.5 ± 0.4 nCi, $n = 15$ ROIs versus 0.4 ± 0.2 nCi, $n = 13$ ROIs, $p < 0.0001$) (Figure 4B). IHC displayed positive TRA staining (Figure 4C) in areas of tracer accumulation. An analysis upon coregistration of the TRA IHC and autoradiographs exhibited a strong, positive association ($r = 0.69$) (Figure 4D) wherein higher tracer uptake directly correlated with high TRA expression.

Patient IHC Analysis.

To establish clinical relevance, we probed for TRA expression using unmodified Bsg in various malignant and benign tissues obtained from patients. In TRA+ embryonal carcinoma, Bsg staining displayed high TRA expression compared to staining with a control, nonspecific IgG (Figure 5A), indicative of specificity of the antibody. In a panel of tumor tissues (Figure 5B–E, Table 1), the highest Bsg staining was observed in gastric cancer with 100% of tissue samples staining positive. Endometrial cancer displayed 86% positive staining, followed by prostate cancer with 55%. Ovarian (43%), pancreatic (41%),

and breast (38%) carcinoma showed moderate TRA expression, whereas colon and lung (squamous and adenocarcinoma) had the lowest expression. Of note, metastatic prostate (Figure 5F, left) and colon (Figure 5F, right) had higher Bsg staining. Benign tissues (e.g., cardiac, bone, and peripheral nerve) showed minimal to no staining. (Figure S4A). Normal pancreatic tissue exhibited focal staining between 0 and 10% (Figure S4B, right), while tubule staining (1%, Figure S4B left) was observed in all benign kidney tissues.

DISCUSSION

Our work herein laid down the development and preclinical evaluation of an imaging tracer for a different yet novel tumor-initiating target, TRA-1–60, also a known marker of pluripotent stemness as established by the Cancer Stem Cell Initiative.[30] The rationale and significance of our work stemmed from the study reported by our group, which centered on the pathological analysis of the expression of TRA-1–60 and other markers of pluripotency and tumor initiation in primary prostate cancer patient tissues. TRA-1–60 was highly expressed in 13% of the high-grade and 9% of the low-grade tumors, suggesting that these high-grade tumors with increased staining correlated with cases that can potentially develop into metastatic disease.[9] Indeed, several groups have proven the tumorigenicity of TRA-1–60+ sorted prostate[14] and treatment-refractory follicular lymphoma cells,[5] establishing this antigen as a driver of tumor initiation. These seminal works, together with the minimal imaging agents in this space, clearly underscores the need for the development of a noninvasive TRA-1–60 immunoPET agent for *in situ* identification of patient populations with a high likelihood for metastasis and tumor initiation. From our perspective, [^{89}Zr]Zr-DFO-Bsg is a preliminary step to bridge this unmet clinical need.

To the best of our knowledge, [^{89}Zr]Zr-DFO-Bsg is the first imaging probe developed to target TRA+ tumors. We established proof-of-principle studies demonstrating specific detection of high versus low TRA-expressing tumors via [^{89}Zr]Zr-DFO-Bsg PET. This was supported by the low tumor accumulation of the nonspecific radiolabeled IgG, and a positive relationship shown between the accumulation of [^{89}Zr]Zr-DFO-Bsg from autoradiographs and TRA expression from the IHC. We have further proven that TRA is membranous with colocalization of the Cy5.5-conjugated Bsg through *in vitro* imaging, making it a viable extracellular target for antibody-based therapeutic and detection payloads. While expression of the antigen in 2D cultures appear minimal and may look clinically insignificant, it does not recapitulate our findings in xenografts and patient tumor tissues with established tertiary structures. Histopathological examination of TRA expression in a number of tissue samples exhibited positive Bsg staining in primary malignancies with stronger staining displayed in metastatic lesions. The high percentages of strongly positive Bstrongomab staining identified in various malignant tissues underscore the broad applicability of a TRA-1–60 targeted tracer.

The tissue distribution studies exhibited correlation with the imaging data; however, improved pharmacokinetics, specifically for blood clearance, is warranted. Modifications on the antibody are underway to address this issue. The competitive inhibition seemed inadequate even with ~100-fold addition of unmodified Bsg with normalized tissue weights (%ID/g). This likely stems from the shedding of TRA into the blood, a phenomenon that has

been previously reported in germ cell tumors.[6,17] Of note, insufficient blocking has also been observed with other shed antigens. In the case of a CA19.9 immunoPET imaging, blocking of [^{89}Zr]Zr-hu5B1 accumulation in BxPC-3 pancreatic tumors with excess hu5B1 antibody was unsuccessful when normalized for tissue weight (%ID/g) but proven blocked when accounting only for injected radioactivity (%ID).[24] Another plausible explanation can be derived from the glycosylation structure of TRA forming repeat tetracarbohydrate units (targeted by Bsg) on numerous sites of podocalyxin, its protein anchor.[7,8] This polymeric structure likely has multiple epitopes, which can require higher doses to saturate. Nevertheless, analysis of the blocked versus unblocked cohorts without accounting for tissue weight revealed a 6.7-fold lower probe accumulation in the blocked groups. Additionally, the tumor to blood ratio decreased between the unblocked (0.73) and the blocked cohorts (0.56), suggestive of moderate blocking of the target epitope.

Taken collectively, we have demonstrated the potential of [^{89}Zr]Zr-DFO-Bsg to delineate TRA+ malignancies. TRA immunoPET can potentially be utilized as a tool to select patients who can benefit from targeted therapy.

Supplementary Material

Refer to Web version on PubMed Central for supplementary material.

ACKNOWLEDGMENTS

We would like to thank Lisa Polin, PhD and Jessica Back, PhD for helpful technical discussions and Agnes Malysa for technical support.

Funding

JMW is supported by the National Institutes of Health under award number NIH T32-CA009531. The Microscopy, Imaging, and Cytometry Resources Core (MICR) is supported, in part, by the NIH Cancer Center Grant No. P30 CA022453 to the Karmanos Cancer Institute at Wayne State University, and the Perinatology Research Branch of the National Institutes of Child Health and Development at Wayne State University.

REFERENCES

(1). Dagogo-Jack I; Shaw AT Tumour Heterogeneity and Resistance to Cancer Therapies. Nat. Rev. Clin. Oncol 2018, 15 (2), 81–94. [PubMed: 29115304]

(2). Gasch C; Ffrench B; O'Leary JJ; Gallagher MF Catching Moving Targets: Cancer Stem Cell Hierarchies, Therapy-Resistance & Considerations for Clinical Intervention. Mol. Cancer 2017, 16, 43. [PubMed: 28228161]

(3). Mitra A; Mishra L; Li S EMT, CTCs and CSCs in Tumor Relapse and Drug-Resistance. Oncotarget 2015, 6 (13), 10697–10711. [PubMed: 25986923]

(4). Reya T; Morrison SJ; Clarke MF; Weissman IL Stem Cells, Cancer and Cancer Stem Cells. Nature 2001, 414 (6859), 105–111. [PubMed: 11689955]

(5). Takata K; Saito K; Maruyama S; Miyata-Takata T; Iioka H; Okuda S; Ling Y; Karube K; Miki Y; Maeda Y; et al. Identification of TRA-1–60-Positive Cells as a Potent Refractory Population in Follicular Lymphomas. Cancer Sci 2018, 110 (1), 443–457. [PubMed: 30417470]

(6). Malecki M; Anderson M; Beauchaine M; Seo S; Tombokan X; Malecki R TRA-1–60+, SSEA-4+, Oct4A+, Nanog+ Clones of Pluripotent Stem Cells in the Embryonal Carcinomas of the Ovaries. J. Stem Cell Res. Ther 2012, 2 (5), 130. [PubMed: 23293749]

(7). Natunen S; Satomaa T; Pitkänen V; Salo H; Mikkola M; Natunen J; Otonkoski T; Valmu L The Binding Specificity of the Marker Antibodies Tra-1–60 and Tra-1–81 Reveals a Novel

Pluripotency-Associated Type 1 Lactosamine Epitope. Glycobiology 2011, 21 (9), 1125–1130. [PubMed: 21159783]

(8). Schopperle WM; DeWolf WC The TRA-1–60 and TRA-1–81 Human Pluripotent Stem Cell Markers Are Expressed on Podocalyxin in Embryonal Carcinoma. Stem Cells 2007, 25 (3), 723–730. [PubMed: 17124010]

(9). Heath EI; Heilbrun LK; Smith D; Schopperle WM; Ju Y; Bolton S; Ahmed Q; Sakr WA Overexpression of the Pluripotent Stem Cell Marker Podocalyxin in Prostate Cancer. Anticancer Res. 2018, 38 (11), 6361–6366. [PubMed: 30396958]

(10). Andrews PW; Banting G; Damjanov I; Arnaud D; Avner P Three Monoclonal Antibodies Defining Distinct Differentiation Antigens Associated with Different High Molecular Weight Polypeptides on the Surface of Human Embryonal Carcinoma Cells. Hybridoma 1984, 3 (4), 347–361. [PubMed: 6396197]

(11). Andrews PW; Casper J; Damjanov I; Duggan-Keen M; Giwercman A; Hata J; von Keitz A; Looijenga LHJ; Millan JL; Oosterhuis JW; et al. Comparative Analysis of Cell Surface Antigens Expressed by Cell Lines Derived from Human Germ Cell Tumours. Int. J. Cancer 1996, 66 (6), 806–816. [PubMed: 8647654]

(12). Wright AJ; Andrews PW Surface Marker Antigens in the Characterization of Human Embryonic Stem Cells. Stem Cell Res. 2009, 3 (1), 3–11. [PubMed: 19398226]

(13). Badcock G; Pigott C; Goepel J; Andrews PW The Human Embryonal Carcinoma Marker Antigen TRA-1–60 Is a Sialylated Keratan Sulfate Proteoglycan. Cancer Res. 1999, 59 (18), 4715–4719. [PubMed: 10493530]

(14). Rajasekhar VK; Studer L; Gerald W; Socci ND; Scher HI Tumour-Initiating Stem-like Cells in Human Prostate Cancer Exhibit Increased NF-KB Signalling. Nat. Commun 2011, 2 (1), 162. [PubMed: 21245843]

(15). Kim W-T; Ryu CJ Cancer Stem Cell Surface Markers on Normal Stem Cells. BMB Rep 2017, 50 (6), 285–298. [PubMed: 28270302]

(16). Saukkonen K; Hagström J; Mustonen H; Juuti A; Nordling S; Fermér C; Nilsson O; Seppänen H; Haglund C Podocalyxin Is a Marker of Poor Prognosis in Pancreatic Ductal Adenocarcinoma. PLoS One 2015, 10 (6), No. e0129012. [PubMed: 26053486]

(17). Marrink J; Andrews PW; Van Brummen PJ; De Jong HJ; Sleijfer DTH; Schraffordt Koops H; Oosterhuis JW Tra-1–60: A New Serum Marker in Patients with Germ-Cell Tumors. Int. J. Cancer 1991, 49 (3), 368–372. [PubMed: 1717384]

(18). Andrews PW Retinoic Acid Induces Neuronal Differentiation of a Cloned Human Embtyonal Carcinoma Cell Line in Vitro. Dev. Biol 1984, 103, 285–293. [PubMed: 6144603]

(19). Adewumi O; Aflatoonian B; Ahrlund-Richter L; Amit M; Andrews PW; Beighton G; Bello PA; Benvenisty N; Berry LS; Bevan S; et al. Characterization of Human Embryonic Stem Cell Lines by the International Stem Cell Initiative. Nat. Biotechnol 2007, 25 (7), 803–816. [PubMed: 17572666]

(20). Levina V; Marrangoni AM; DeMarco R; Gorelik E; Lokshin AE Drug-Selected Human Lung Cancer Stem Cells: Cytokine Network, Tumorigenic and Metastatic Properties. PLoS One 2008, 3 (8), No. e3077. [PubMed: 18728788]

(21). McKnight BN; Kuda-Wedagedara ANW; Sevak KK; Abdel-Atti D; Wiesend WN; Ku A; Selvakumar D; Carlin SD; Lewis JS; Viola-Villegas NT Imaging EGFR and HER3 through 89Zr-Labeled MEHD7945A (Duligotuzumab). Sci. Rep 2018, 8 (1), 9043. [PubMed: 29899472]

(22). Zeglis BM; Lewis JS The Bioconjugation and Radiosynthesis of 89Zr-DFO-Labeled Antibodies. J. Visualized Exp 2015, 96.

(23). Brand C; Sadique A; Houghton JL; Gangangari K; Ponte JF; Lewis JS; Pillarsetty NVK; Konner JA; Reiner T Leveraging PET to Image Folate Receptor α Therapy of an Antibody-Drug Conjugate. EJNMMI Res. 2018, 8 (1), 87. [PubMed: 30155674]

(24). Viola-Villegas NT; Rice SL; Carlin S; Wu X; Evans MJ; Sevak KK; Drobjnak M; Ragupathi G; Sawada R; Scholz WW; et al. Applying PET to Broaden the Diagnostic Utility of the Clinically Validated CA19.9 Serum Biomarker for Oncology. J. Nucl. Med 2013, 54 (11), 1876–1882. [PubMed: 24029655]

(25). Lindmo T; Boven E; Cuttitta F; Fedorko J; Bunn PA Determination of the Immunoreactive Function of Radiolabeled Monoclonal Antibodies by Linear Extrapolation to Binding at Infinite Antigen Excess. J. Immunol. Methods 1984, 72 (1), 77–89. [PubMed: 6086763]

(26). Holland JP; Divilov V; Bander NH; Smith-Jones PM; Larson SM; Lewis JS; Phil D Zr-DFO-J591 for ImmunoPET Imaging of Prostate-Specific Membrane Antigen (PSMA) Expression in Vivo. J. Nucl. Med 2010, 51 (8), 1293–1300. [PubMed: 20660376]

(27). Anderson CJ; Schwarz SW; Connett JM; Cutler PD; Guo LW; Germain CJ; Philpott GW; Zinn KR; Greiner DP; Meares CF Preparation, Biodistribution and Dosimetry of Copper-64-Labeled Anti-Colorectal Carcinoma Monoclonal Antibody Fragments 1A3-F(Ab')2. J. Nucl. Med 1995, 36 (5), 850–858. [PubMed: 7738663]

(28). Verel I; Visser GWM; Boellaard R; Stigter-van Walsum M; Snow GB; van Dongen GAMS 89Zr Immuno-PET: Comprehensive Procedures for the Production of 89Zr-Labeled Monoclonal Antibodies. J. Nucl. Med 2003, 44 (8), 1271–1281. [PubMed: 12902418]

(29). Wu AM Engineered Antibodies for Molecular Imaging of Cancer. Methods 2014, 65 (1), 139–147. [PubMed: 24091005]

(30). Adewumi O; Aflatoonian B; Ahrlund-Richter L; Amit M; Andrews PW; Beighton G; Bello PA; Benvenisty N; Berry LS; Bevan S; et al. Characterization of Human Embryonic Stem Cell Lines by the International Stem Cell Initiative. Nat. Biotechnol 2007, 25 (7), 803–816. [PubMed: 17572666]

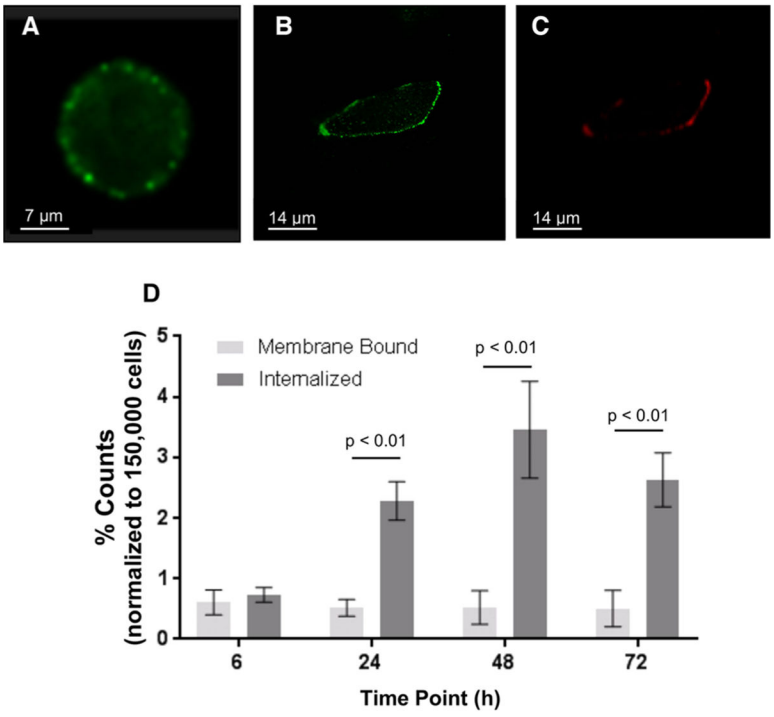

Figure 1.

In vitro imaging of TRA in BxPC-3 by (A) single cell imaging flow cytometry and (B) confocal imaging with TRA-1–60-AF488. (C) Counterstain with Bsg-cy5.5 showed localization of the probe on the cell surface. All confocal images were captured in 63×.(D) [^{89}Zr]Zr-DFO-Bsg exhibited internalization with the high TRA-expressing NCCIT embryonal carcinoma cell line.

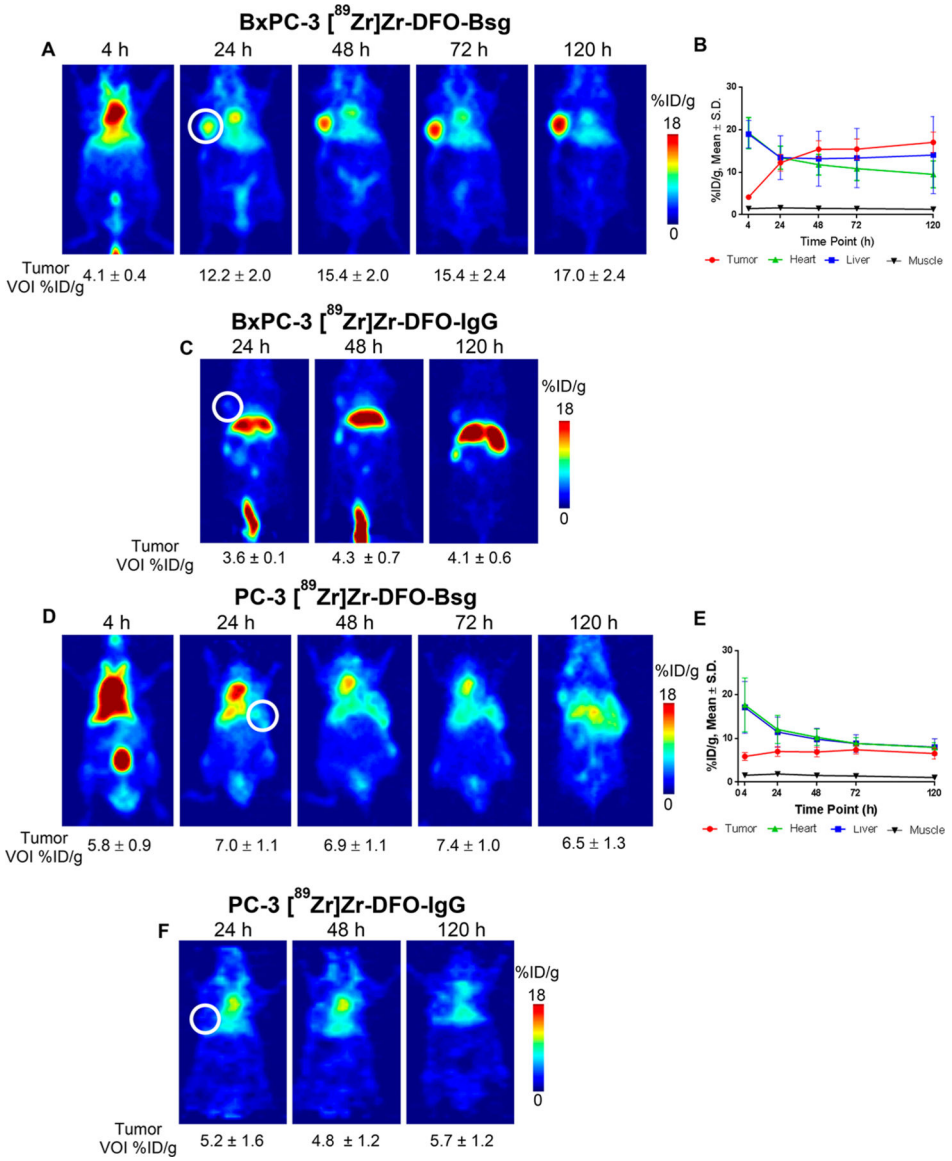

Figure 2.

(A) *In vivo* PET 2D slices of BxPC-3 xenografts imaged with [^{89}Zr]Zr-DFO-Bsg from 4 to 120 h p.i. (B) Time activity curve of [^{89}Zr]Zr-DFO-Bsg injected mice examines tumor, heart, liver, and muscle uptake from 4 to 120 h. (C) [^{89}Zr]Zr-DFO-IgG imaging of mice for comparison of nonspecific uptake and EPR effect. (D) PC-3 xenografted mice imaged with [^{89}Zr]Zr-DFO-Bsg from 4–120 h p.i. with (E) time activity curve uptake and the (F) [^{89}Zr]Zr-DFO-IgG comparison. Tumors are marked by the white circle.

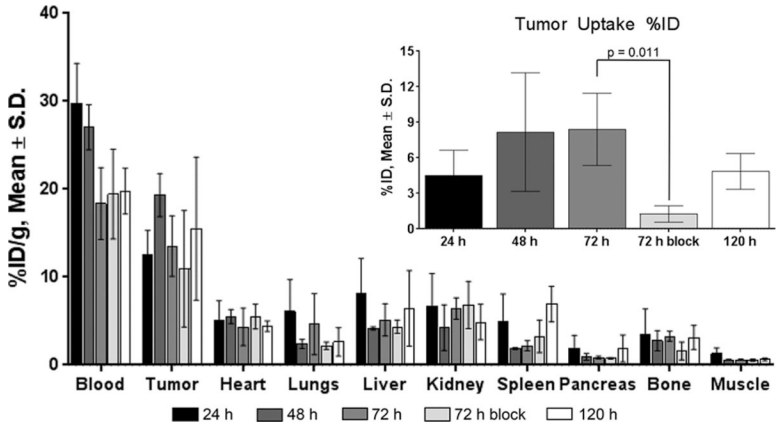

Figure 3.

Tissue uptake of [^{89}Zr]Zr-DFO-Bsg in BxPC-3 tumor bearing mice at 24, 48, 72, and 120 h p.i. time points ($n \geq 3$). A competitive dose of excess ~500 μg nonradiolabeled antibody was coinjected with the tracer with the tissue uptake measured at 72 h p.i. The inset shows %ID tumor uptake from 24 to 120 h p.i. Tracer uptake was significantly higher in the 72 h unblocked cohort compared to the 72 h blocked cohort ($p = 0.011$). Error bars represent S.D.

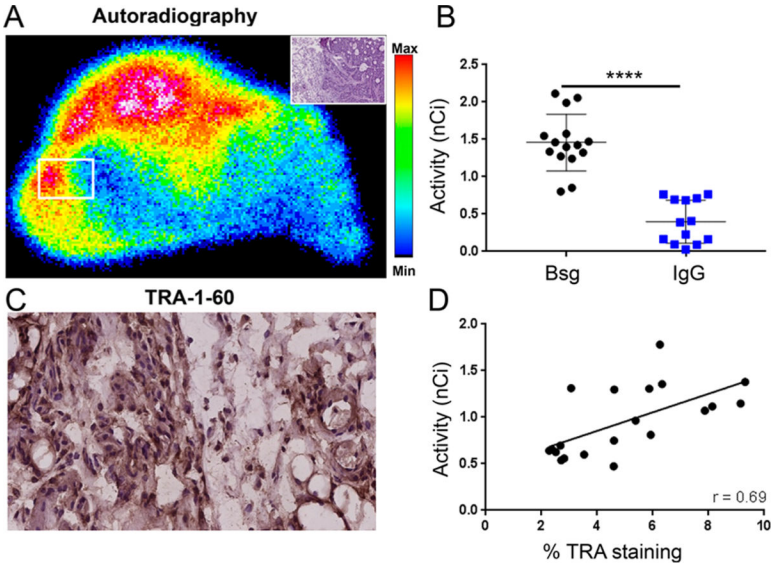

Figure 4.

BxPC-3 tumors were resected from mice following immunoPET imaging for autoradiography and immunohistochemical analyses. (A) *Ex vivo* autoradiography of BxPC-3 demonstrated focal uptake. The white box displays the area where tracer uptake was measured. Inset: H&E staining of representative area. (B) Comparison of tracer accumulation in tumors (nCi) from autoradiographs of [^{89}Zr]Zr-DFO-Bsg and [^{89}Zr]Zr-DFO-IgG. (C) Immunohistochemistry of tumor sections (5 μm, 400×) exhibited TRA expression. (D) Spearman correlation analysis comparing tracer uptake in the tumor (nCi) versus %TRA-1–60 staining by IHC showed a positive correlation. Error bars represent SD ****p <0.0001.

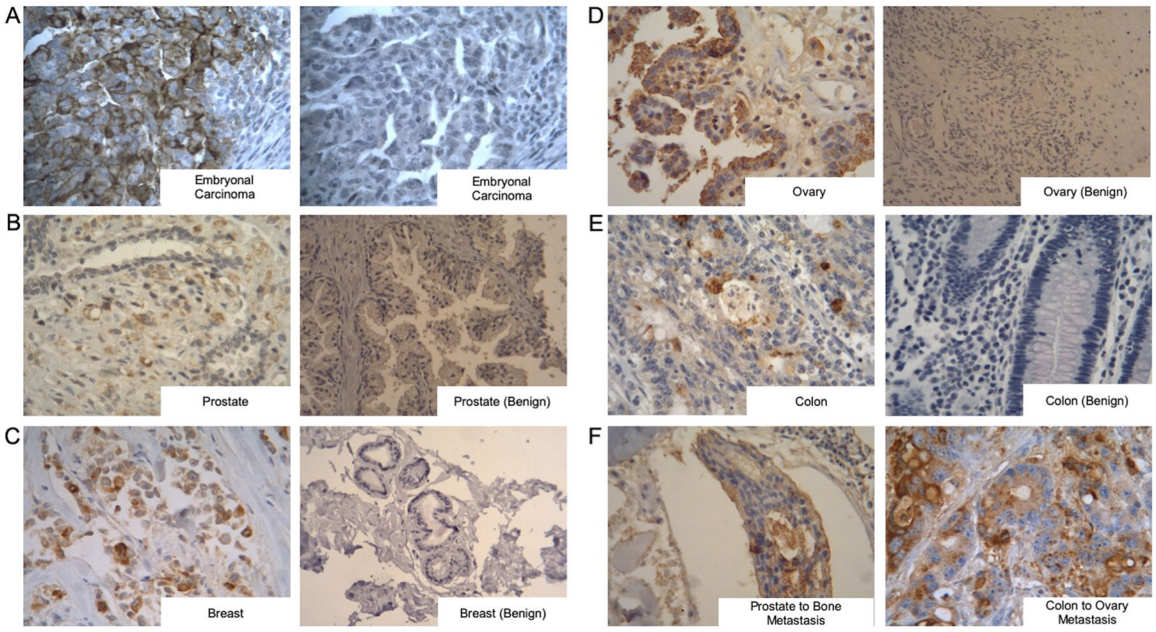

Figure 5.

Bstrongomab immunohistochemical staining of benign and malignant tissues. (A) Embryonal carcinoma demonstrates positive staining with Bstrongomab (left) compared to a nonspecific isotype control (right). (B–E) Comparison of TRA expression in primary cancerous tissues (left) compared to benign (right) samples of (B) prostate, (C) breast, (D) ovarian, and (E) colon. (F) Presence of TRA-1–60 was examined in metastatic prostate (left) and metastatic colon (right) carcinomas. Benign prostate, benign breast, and benign ovarian images are 200×, all other images are 400×.

Table 1.

TRA IHC Expression from Primary Carcinoma Solid Tumors

primary carcinoma	total # patients	% strong positive Bstrongomab
pancreatic	38	41%
prostatic	38	55%
breast	149	38%
ovarian	30	43%
gastric	8	100%
endometrium	8	86%
colon	30	30%
lung	66	25% squamous cancer, 30% adenocarcinoma